International Journal of Occupational Safety and Health

ISSN: 2091-0878 (Online) ISSN: 2738-9707 (Print)

Short Communication

OpenFOAM Analysis on the Comparison of Safety Requirements Provided for Water-Air and LOX-He Storage Systems

Sarath Raj[1,2,3], Bibin Kattupurathu Scharia[2,4], Reby Roy Krishnan Kutty Elsy Bai[1]

[1]Department of Mechanical Engineering, T.K.M. College of Engineering, A.P.J. Abdul Kalam Technological University, Kollam-691005, Kerala, India,

[2]Department of Mechanical Engineering, Amrita Vishwa Vidyapeetham, Amrita University, Amritapuri-690546, Kerala, India.

[3]Department of Mechanical Automobile Engineering, Sree Narayana Institute of Technology, A.P.J. Abdul Kalam Technological University, Adoor-691554, Kerala, India.

[4]Department of Mechanical Engineering, Mangalam College of Engineering, A.P.J. Abdul Kalam Technological University, Kottayam-686631, Kerala, India.

Corresponding author:

Dr. Raj Sarath,
Post Doctoral Research Fellow,
A.P.J. Abdul Kalam Technological University,
Department of Mechanical Engineering, T.K.M. College of Engineering,
Kollam-691005, Kerala, India,
Tel.: +91-9747334672
In collaboration with the Solenic Medical, Inc.4275 Kellway | Suite 146 | Addison, TX, USA, 75001
E-mail: srsnit2013@gmail.com
ORCID: https://orcid.org/0000-0002-9782-9653

Date of submission: 17.01.2024
Date of acceptance: 03.06.2024
Date of publication: 01.10.2024

Conflicts of interest: None
Supporting agencies: None
DOI: https://doi.org/10.3126/ijosh.v14i4.57612

ABSTRACT

Introduction: In storage vessels filled with cryogenic liquids thermal destratification can be effectively done by the continuous supply of bubble movements. Therefore, the pressure builds up subsequent blasting of such containers can be avoided and cryogenic storage vessels can be used safely. The Volume of Fluid (VOF) approach is utilized in the current computational analysis to examine the safety precautions, dynamics of bubble creation, and subsequent collapse of the free liquid surface in both vertically and horizontally aligned rectangular containers.

Methods: In the present work, using the Volume of Fluid (VOF) method, numerically investigated the sloshing behavior within a rectangular container with a 15% free air space with double gas inlets.

Results: The impact of inlet gas velocity on sloshing rate due to bubbling is investigated numerically. Also, comparative studies are carried out to investigate the variations of bubble diameter, detachment time, and bubble detachment frequencies considering water-air and LOX-He systems. The mixing behaviors in liquid oxygen (LOX) due to helium bubble formation under different inlet gas velocities were also numerically investigated. The numerical results show that the average deformation index increased by 23.83% when the water-air system was replaced with the LOX-He system. Hence, it can be understood that for the storage vessels filled with cryogenic liquids more safety precautions have to be considered to avoid thermal stratification. The safety precautions include increasing the gas flow rate and including more number gas flow inlets.

Conclusion: The present analysis concludes that under a given condition the free liquid surface deformation is more for the case where storage vessels filled with LOX-He. Hence, it can be understood that for the storage vessels filled with cryogenic liquids more safety precautions have to be considered to avoid thermal stratification. The safety precautions include increasing the gas flow rate and including more number gas flow inlets.

Keywords: Deformation index; LOX-He; Safety; Storage vessels; Thermal destratification

Introduction

In a variety of scientific and engineering domains, the phenomenon of bubble generation from submerged gas inlets and bubbly flows occurring in different equipment are issues of interest.[1,2] This comprises direct-contact heat exchangers, fluidized beds, gas-liquid bubble columns, and reactors.[2] Gas-liquid bubble columns and fluidized beds are frequently employed in the chemical, biochemical, and petrochemical industries, as well as in gas-phase polymerization, combustion, drying processes, etc.[2] They come with several benefits, including high heat and mass transfer coefficients at the gas-liquid interface and low operating costs.[1,2] Additionally, gas bubble formation and ensuing agglomeration stir the liquid phase, resulting in enough interphase contact.[2] Thus, to enhance and regulate heat and mass transfer rates, gas bubbles are frequently used in fluidized beds and gas-liquid bubble reactors.[1,2]

Arai et al. performed a numerical analysis to contrast the smoothed particle hydrodynamics (SPH) and Volume of Fluid (VOF) models.[1,2,3] They used various Reynolds numbers (Re) and Morton number (Mo) values for the analysis. It was reported that neither model could forecast the bubble rise velocity for modest Mo values. They concluded that the VOF model is more suitable for investigating different bubble behavior in viscosity-dominated regions. The SPH model eventually captured the variation in viscosity. Experimental evaluations were conducted by Bae et al. to look into the bubble flow pattern in gas-solid fluidized beds. Silicon particles of metallurgical grade were employed as the bed material.[4] They found that the observed bubble diameter value matches Choi et al. correlations.[5] Becker et al. performed the numerical analysis using the commercial computational fluid dynamics tool FLOW3D. Studying bubble behavior under flow boiling circumstances was the primary goal of their investigation. Their findings include information on the relationship between bubble dynamics, heat transfer properties, bulk flow velocity, and wall heat transfer.[6] A cylindrical microbubble vibrating due to pressure oscillations was subjected to a 3-Dimensional numerical study by Behdani et al. They studied that bubbles produce a vortex layer on top of them. The size of the bubble grew due to the vortex formation.[7] Ma et al. carried out the numerical analysis in a vertical rectangular container filled with liquid.[8] By considering different values of liquid densities, and viscosities and by changing the inlet gas flow rate, they investigated different bubble characteristics. A transient model was introduced by Diaz et al. to study the behavior of gas bubbles in oil and refrigerant solutions. The findings showed three stages to the bubble growth process: a gradual growth phase, a rapid bubble expansion, and a third stage where the bubble growth stabilizes.[5,9] Donelly et al. conducted an experimental analysis to determine the impact of heat transfer on bubble sliding movement on heat transfer increases. The investigation found that bubble movement, shape, and velocity oscillations increased with void fraction of the air bubbles. They found hairpin vortices peeling from the back of the bubbles when they studied the bubble movement down the heated sloped surface.[10] Sarath and Jayakumar carried out numerical investigations of thermal and flow characteristics over a forward-facing step. Considering different values of aspect ratios, inlet mass flow rate, and considering different liquids they compared variations in flow separation occurring both at upstream and downstream regions.[11,26] Using various bubble characters, Sarath and Jayakumar investigated thermal destratification in the 3D cylindrical domain. Changing inlet gas flow rate, considering different values of orifice diameters (D_o), they studied variation in thermal destratification. They quantified thermal destratification in terms of the newly defined parameter the destratification index. They found that the destratification index increased with an increase in average bubble diameter.[12,13]

In cryogenic propellent tanks filled with liquid oxygen, liquid nitrogen, liquified natural gas, etc., even though proper insulations are provided

there are possibilities of thermal stratification caused by external heat infiltration. Due to this external heat infiltration, the liquid near the storage vessel wall is heated up. Hence, the temperature of liquid stored in the vessel no longer will be uniform.[13] Therefore, a stratified temperature layer will form.[12] And continuous heat leakage in the uppermost liquid layer will reach a maximum temperature, beyond the saturation temperature of cryogenic liquid.[12,13] Hence the liquid near the ullage area of storage vessels becomes vaporized and the vapor pressure at the ullage area increases.[11-13] Therefore, the upper propellant near the ullage area experiences relatively larger vapor pressure, which affects aspects like tank pressure and structural stability.[12,13] Hence propellant tanks under exposure to an external heat source become more pressurised quickly than without stratification.[12] Destratification of the temperature layer is the only way to bring the pressure at the ullage area to the working safe pressure.[11] Thermal destratification by the movement of bubbles breaks the stratified temperature layer and mixes different temperature layers to create a uniform safe working temperature.[12]

The VOF technique was used in the current work to simulate the free liquid collapse and the performance characteristics of 2-Dimensional bubbling.[14] The simulations are run in containers with the axis vertically aligned.[11,27] In a 2D domain with a double inlet case, bubble behavior was the subject of the simulation. No published comparison studies have been reported on bubble dynamics in a 2D vertically aligned rectangular domain with gas intakes filled with liquid oxygen (LOX).[5] This work investigates various bubble behavior variations under different incoming gas velocities.[15,16] Using computer simulations, the bubble diameter, bubble agglomeration, and bubble detachment time were all specifically examined.[11] The simulation also considered the role of input gas velocity in the free-surface collapsing in the rectangular containers.[5] Comparative studies are carried out to investigate the variations of bubble diameter, detachment time, and bubble detachment frequencies considering water-air and LOX-He systems.[17] The mixing behaviors in LOX due to helium bubble formation under different inlet gas velocities were also numerically investigated. Introducing a dimensionless number, the deformation index, the free liquid surface deformation due to the bubble bursting is quantified both in water-air and LOX-He system. Measuring the free liquid surface deformation due to the bubble bursting helps in designing a cryogenic liquid storage system that will work without creating hazardous phenomena.[18,19,20] Also, by measuring the free liquid surface deformation due to bubble bursting thermal destratification can be done in storage vessels and hence the inlet mass flow rate of gas-producing bubbles can be controlled. In storage vessels filled with cryogenic liquids thermal destratification can be effectively done by a continuous supply of bubble movements. Therefore, the pressure builds up and subsequent blasting of such containers can be avoided and cryogenic storage vessels can be used safely.[21,22,23]

Methods

For two-phase flow, the continuity and momentum equations are expressed as follows:[1,2,14]

$$\frac{\partial \rho}{\partial t} + \nabla.(\rho \vec{V}) = 0 \quad (1)$$

In (1), $\vec{V}$ is the relative velocity between the two phases.

$$\frac{\partial(\rho \vec{V})}{\partial t} + \nabla.(\rho \vec{V}\vec{V}) = -\nabla p_{rgh} + \nabla.[\mu(\nabla \vec{V}) + (\nabla \vec{V})^T] + \sigma \nabla \alpha_1 - \vec{g}.\vec{y}\nabla\rho \quad (2)$$

In (2), P_{rgh} is hydrostatic pressure calculated in (3).

$$p_{rgh} = p - \rho \vec{g} \cdot \vec{y} \quad (3)$$

In (3) term p is the total specified system pressure and $\rho \vec{g} \cdot \vec{y}$ is the system static pressure.

In (1), (2) and (3), density and dynamic viscosity are calculated using (4) and (5).

$$\rho = \rho_1 \alpha_1 + \rho_2 (1 - \alpha_1) \quad (4)$$

$$\mu = \mu_1 \alpha_1 + \mu_2 (1 - \alpha_1) \quad (5)$$

A single set of momentum and volume fraction equations applies to all the fluids in the VOF scheme. As a result, equations (6) and (7) are used to trace the computational grid across the entire domain.[16]

$$\alpha = \frac{Volume\ of\ fluid\ in\ unit}{Volume\ of\ unit} \quad (6)$$

$$\alpha = \begin{cases} 0 & Inbubble \\ 0 < \alpha < 1 & Interface \\ 1 & In\ liquid\ fluid \end{cases} \quad (7)$$

The transport equation of the fluid volume function (8) is used by the interFoam solver. The solver applies equations (9) to determine the surface tension force at the fluid interface.[13,14,15]

$$\frac{\partial \alpha}{\partial t} + \nabla.(\alpha \vec{v}_r) + \nabla.[\alpha \vec{v}_r(1-\alpha)] = 0 \quad (8)$$

The surface tension force at the liquid gas interface is calculated using (9),

$$F_s = \sigma \frac{\alpha_l \rho_l k_v \nabla \alpha_v + \alpha_v \rho_v k_l \nabla \alpha_l}{0.5(\delta_v + \delta_v)} \quad (9)$$

Where k_l and k_v are the curvature at the gas-liquid interface, which is calculated with (10)

$$k_l = k_g = -\nabla.\hat{r} = -\nabla.\left(\frac{\nabla \alpha_l}{|\nabla \alpha_l|}\right) \quad (10)$$

where $\hat{r}$ is the unit vector normal to the interface.

In the present simulation, the solver interFoam utilizes a surface compression scheme to sharpen the interface (reconstruction of gas-liquid interface)[17,18].

Solver interFoam defines the velocity of the single fluid mixture $\vec{V}$ as

$$\vec{V} = \alpha_l \vec{V}_l + \alpha_g \vec{V}_g = \alpha_l \vec{V}_l + (1-\alpha_l)\vec{V}_g \quad (11)$$

where α_l represents the void fraction of phase 1[17, 18]

The relative velocity between two phases ($\vec{V}_r$) is calculated with (11),

$$\vec{V}_r = \vec{V}_l - \vec{V}_g \quad (12)$$

$\vec{V}_l$ and $\vec{V}_g$ are the velocities of the liquid and gas phases, respectively.

Multiplying Eqn. (11) by α_l and Eqn. (12) by (1- α_l) and adding the results yields the following equation

$$\alpha_l \vec{\boldsymbol{V_l}} = \alpha_l \vec{\boldsymbol{V}} + \alpha_l(1-\alpha_l)\vec{\boldsymbol{V_r}} \quad (13)$$

Substituting equation (13) in the equation for volume fraction (14)[25],

$$\frac{\partial(\alpha_l)}{\partial t} + \nabla.(\alpha_l \vec{V}_l) = 0 \quad (14)$$

Rewriting equation (14) in terms of relative velocity

$$\frac{\partial(\alpha_l)}{\partial t} + \nabla.(\alpha_l \vec{V}) + \nabla.\left[\alpha_l \vec{V}_r(1-\alpha_l)\right] = 0 \quad (15)$$

The surface compression introduced by this new version of the transport equation for volume fraction (Eqn. 15) sharpens the boundary between the liquid and gas phases. The FVM (Finite Volume approach) and VOF approach are the foundation of the OpenFOAM solver interFoam.[14,24,25] The solver includes unique features like adaptive re-meshing and mesh mobility.

The Ma et al.'s numerical works were used to validate the present study's methodology.[8] Figure 1 (a) displays the boundary conditions for the validation task. The relative inaccuracy was less than 5% when comparing the variation in bubble diameter with the inlet gas velocity. The validation result is displayed in Figure 1(b). Figure 1(c) depicts the solution process for the current analysis.

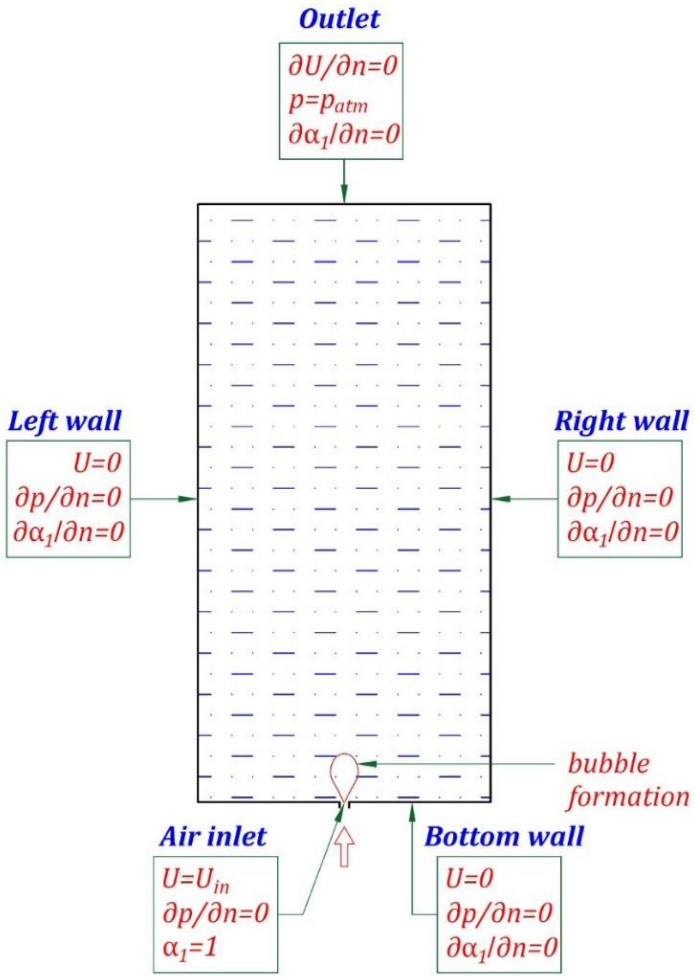
Outlet
∂U/∂n=0
p=p_atm
∂α1/∂n=0
Left wall
U=0
∂p/∂n=0
∂α1/∂n=0
Right wall
U=0
∂p/∂n=0
∂α1/∂n=0
bubble formation
Air inlet
U=U_in
∂p/∂n=0
α1=1
Bottom wall
U=0
∂p/∂n=0
∂α1/∂n=0

(a)

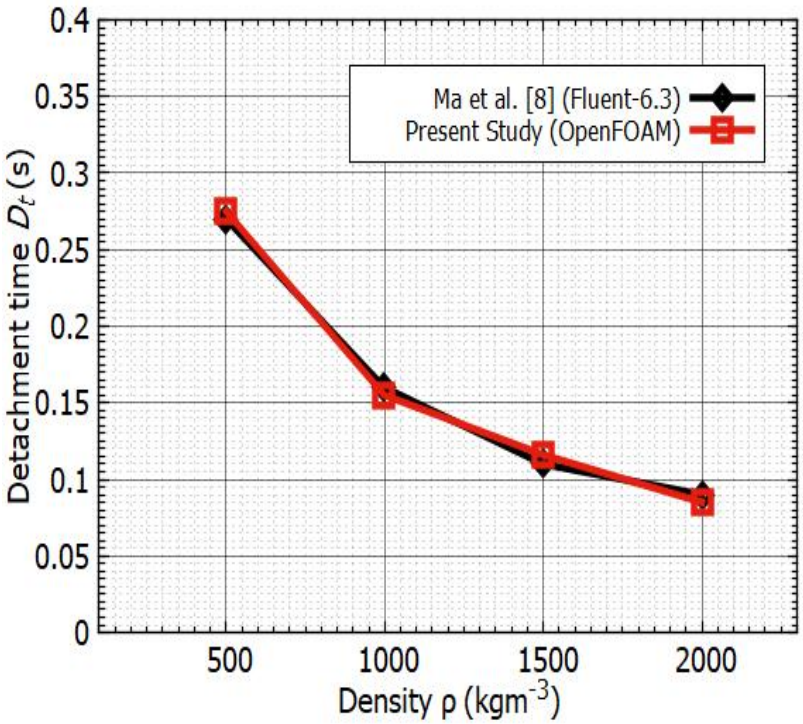
Ma et al. [8] (Fluent-6.3)
Present Study (OpenFOAM)
Detachment time D_t (s)
Density ρ (kgm^{-3})
0
0.05
0.1
0.15
0.2
0.25
0.3
0.35
0.4
500
1000
1500
2000

(b)

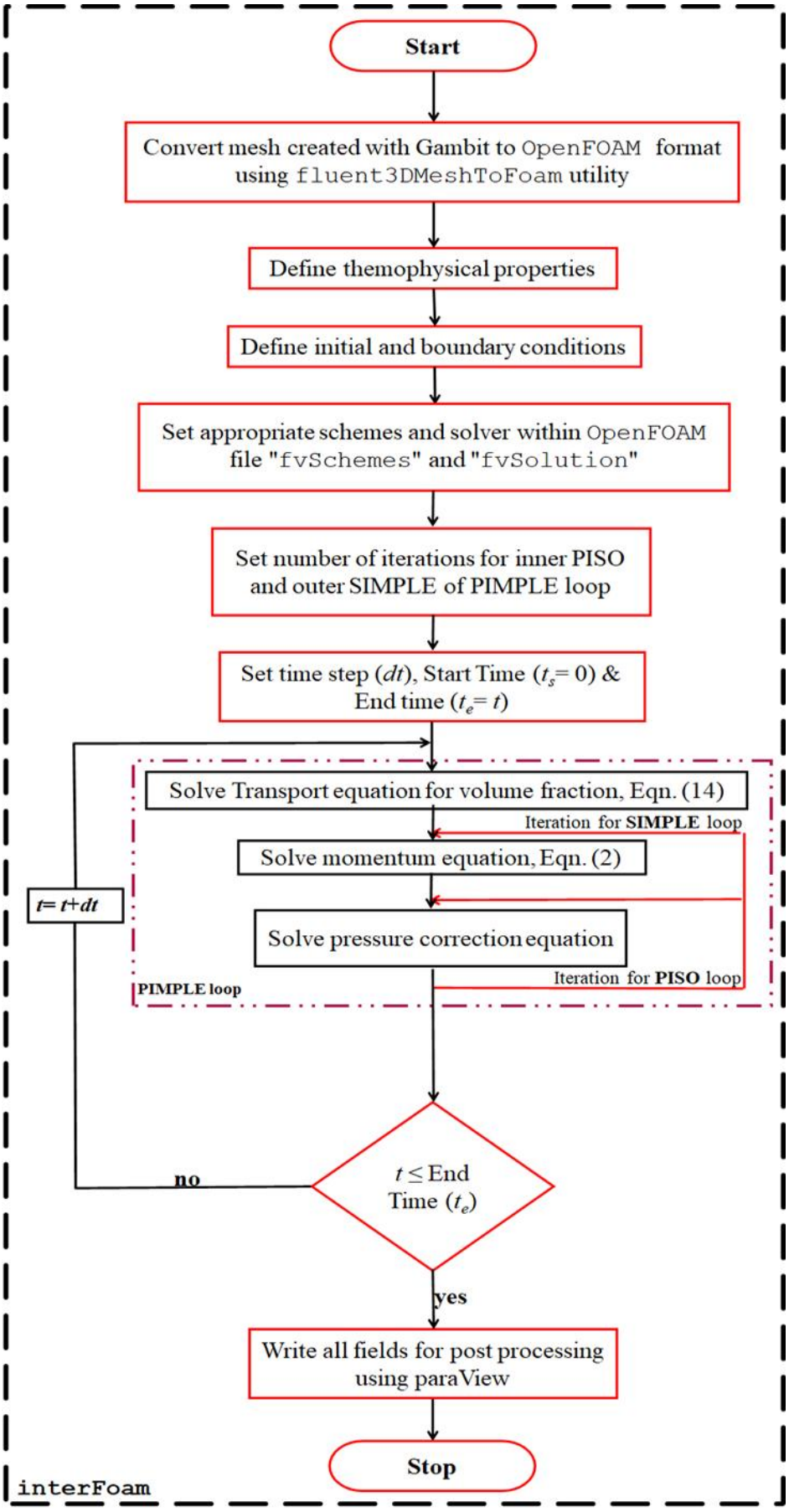

(c)

Figure 1 (a): Boundary conditions and domain for validation; **1 (b):** Variation of bubble detachment time with inlet gas velocity; **1 (c):** Solution procedure

Figure 2 (a) displays the mesh independence research conducted for the current analysis. The 2D computational domain with free air space of 15% and boundary conditions used for the present analysis are shown in Figure 2. (b) and (c). The bulk liquid considered is water and LOX. The gas phase considered is air and helium supplied through the submerged gas inlet of diameter 0.3 mm. The present work is carried out by considering different inlet gas velocities, 0.3, 0.5,0.7, and 0.9 m/s. Acceleration due to gravity g of value 9.81 m/s^2 is considered for the analysis. By varying inlet gas velocity, various bubble behaviors and the variations in the free liquid surface deformation due to the bubble bursting were analyzed. The fluid properties considered for the analyses are shown in Tables 1 and 2.

Table 1: Properties of liquid and gas phase used for the present analysis, Water-Air system

ρ_g(kg/m^3)	ρ_l(kg/m^3)	μ_g(Pa s)	μ_l(Pa s)	σ_l (N/m)
1.225	998.2	1.789e-5	0.001	0.0728

Table 2: Properties of liquid and gas phase used for present analysis, LOX-He system.

ρ_g(kg/m^3)	ρ_l(kg/m^3)	μ_g(Pa s)	μ_l(Pa s)	σ_l (N/m)
0.179	1141	0.00058	1.02e-4	0.02413273

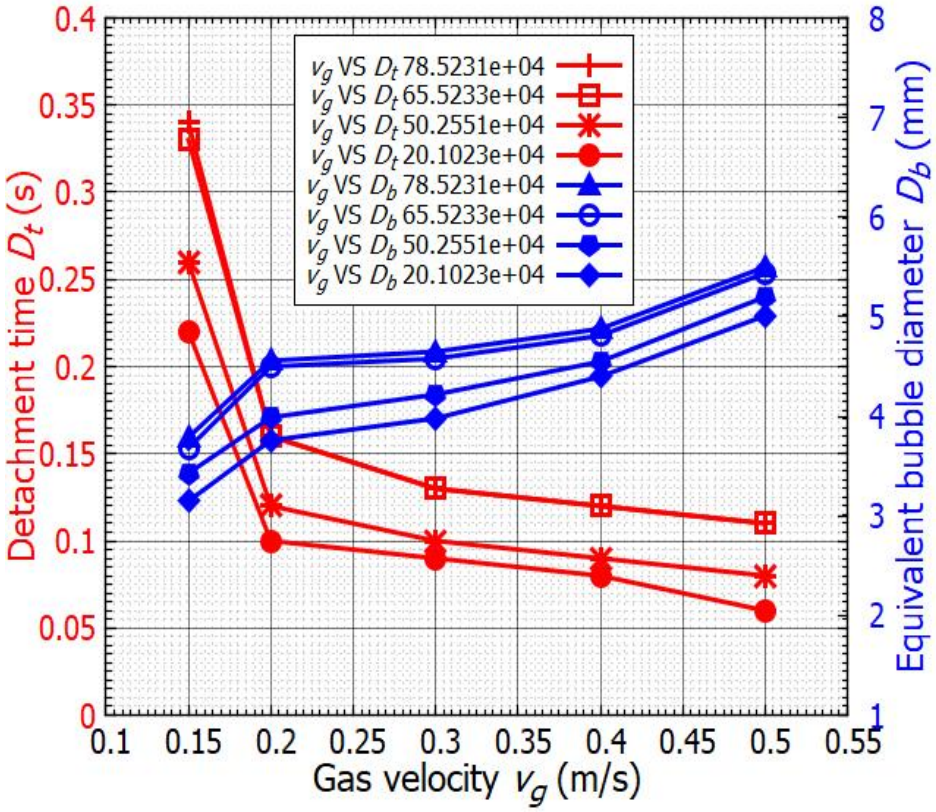

(a)

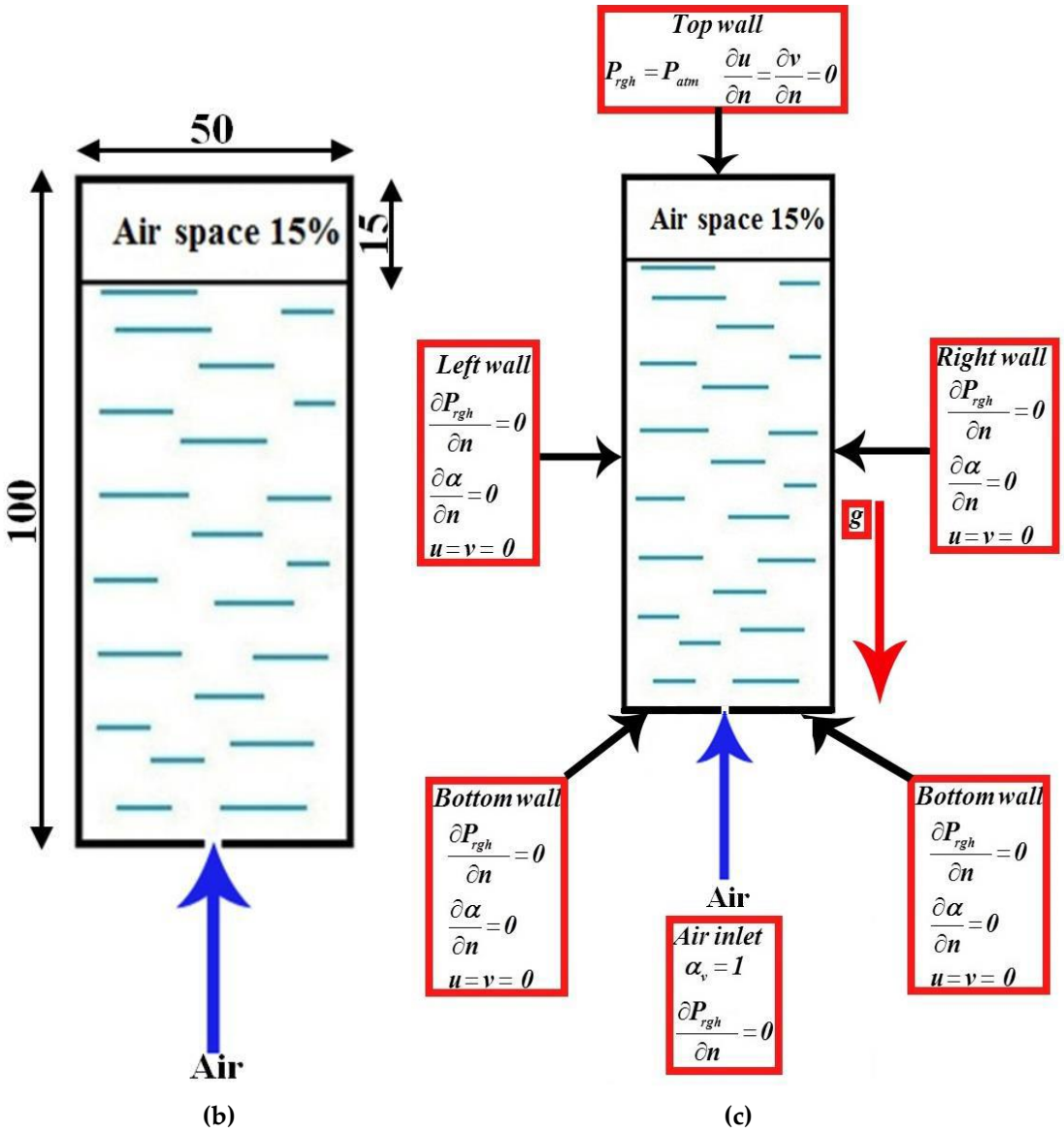

Figure 2 (a): Mesh independency test; **2 (b):** 2D Rectangular domain with double inlets; **2 (c):** Boundary conditions used for the present analysis

Results

This section explains a comparative study of various bubble behaviors and free liquid surface deformation due to the bubble bursting considering water-air and LOX-helium systems. Simulations are carried out by considering different inlet gas velocity (V_g) values viz., 0.3, 0.5, 0.7, and 0.9 m/s. For all the cases the orifice diameter D_o kept constant at 0.3 mm. There are mainly three stages in a bubble life which are as follows, formation (bubble development), neck formation followed by detachment, and finally bubble growth. At the early stage, the newly generated bubble will be attached to the submerged gas inlet by the slender bubble neck. The force of surface tension plays a vital role at this stage. When the buoyancy force dominates the weight of the bubble and external pressure acting on the bubble it gets detached from the orifice. This phenomenon is repeated for the trailing bubbles.

Figures. 3 (a) and (b) show the void fraction contours considering water-air and LOX-helium systems. From the void fraction contours, it is clear that for the water-air system at t= 0.26 s, two bubbles are detached. But for the LOX-helium system at t= 0.26 s four detached bubbles were seen. On comparison from the void fraction contours for other time instants with the LOX-helium system, it is observed that a greater number of bubbles are detached. Hence from the studies, it can be concluded that bubble

detachment frequency increased for the LOX-helium system. Also, the number of bubble coalescence is more for the LOX-helium system. There a greater number of bubbles will be present on the free liquid surface which causes the free liquid surface to rupture more for the LOX-helium system. It is evident that with the increment in time and under the effect of wakes created by the leading bubbles, the relative distance between bubbles gets reduced and ultimately fuses to form a single bubble of larger diameter.

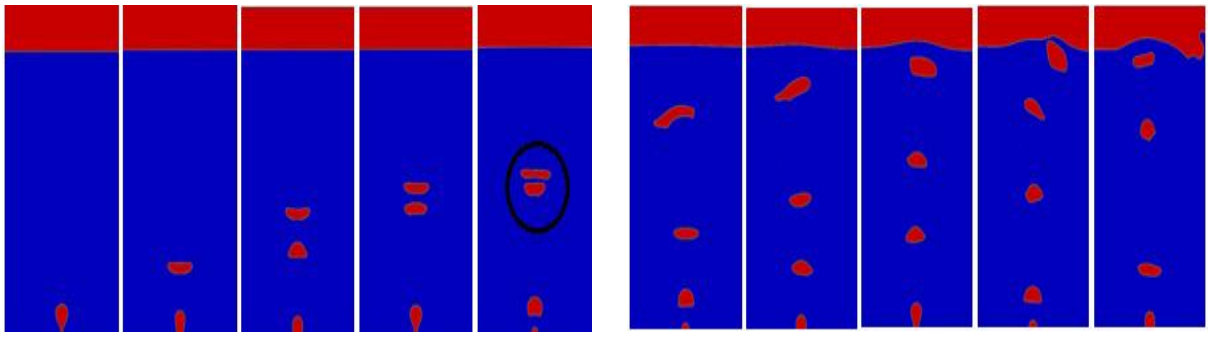

(a): D_o= 0.3 mm, V_g= 0.5 m/s, Water-Air system

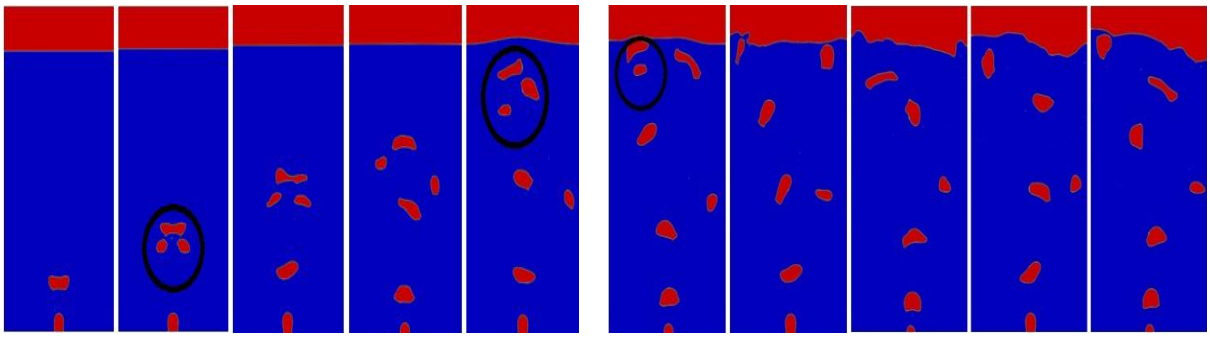

(b): D_o= 0.3 mm, V_g= 0.5 m/s, LOX-He system.

Figure 3: Void fraction contours

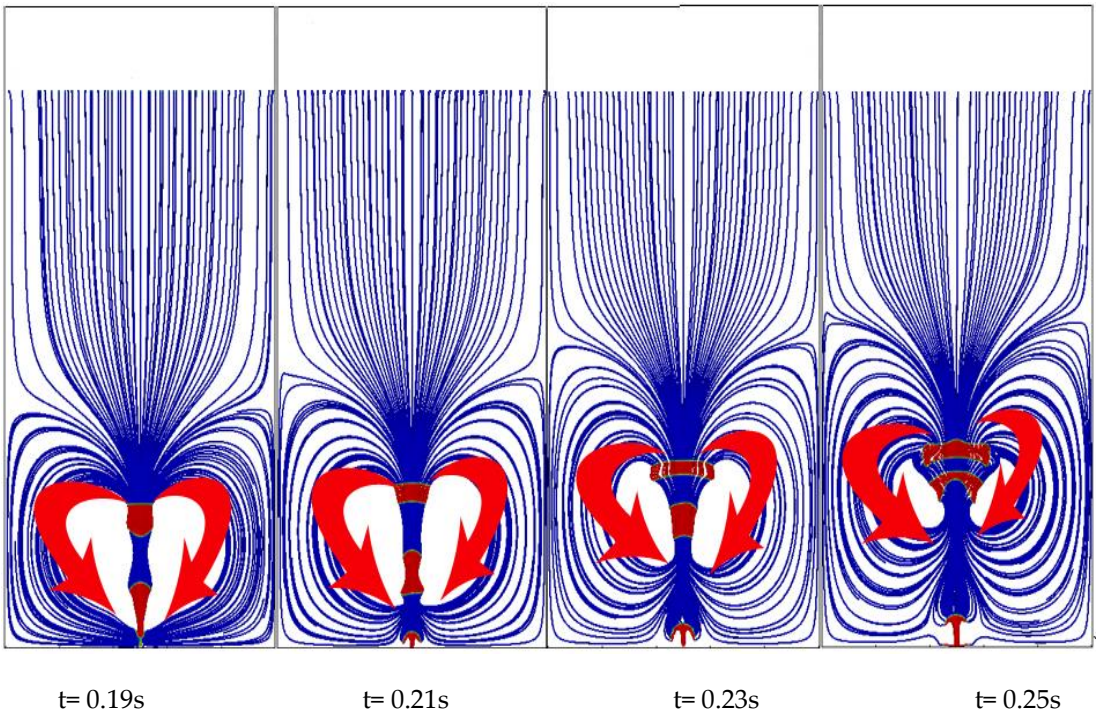

Figure 4: Combined void fraction and streamline contour

To show the effect of wakes created within the bulk liquid due to the bubble movement streamlines are plotted as shown in figure 4. When the leading bubble moves upward through the bulk liquid vortices are created at two sides of the rising bubble as shown in Figure 4. This vortex accelerates the trailing bubble subsequently bubble coalescence takes place. The theory explained matches well with the observations of the work. [1,15]

Discussion

The available literature demonstrates that no studies have considered the specifics of how the gas-liquid interface at the top free liquid surface deforms as a result of bubble formation and bursting while considering LOX-He and Water-air systems. We have examined the deformation of the free liquid surface caused by bubble movement and bursting in the current work, in addition to studying different bubble behaviors. By introducing the deformation coefficient D_L^*, a new metric for measuring the deformation of free liquid surfaces. The ratio of the developed length of the deformed liquid surface at the top air space (L_d) to the storage tank's diameter (D), or the parameter D_L^*, i.e.,

$$D_L^* = \frac{L_d}{D}.$$

The overall curvature length of the deformed liquid surface is added up to determine the developed size of the distorted liquid surface at the top air space (L_d). The value of D_L^*always will be greater than or equal to one ($D_L^* \geq 1$). The value of D_L^* will be 1 if there is no deformation of the top free liquid surface; if $D_L^* > 1$, deformation of the top free liquid surface has occurred. So, measuring the degree of distortion of the free liquid surface is possible using the dimensionless quantity known as the deformation index D_L^*. Utilizing the recently introduced dimensionless parameter D_L^* the deformation of the free liquid surface is measured for LOX-He and Water-air systems.

Figure 5. (a) illustrates the variation in bubble diameter and time of detachment for the systems of water-air and LOX-helium, considering different values of inlet gas velocities. In both the water-air and LOX-helium systems, it is evident from the graph that bubble diameter grows as inlet gas velocity rises. However, LOX-helium systems have higher D_b values. This increase in bubble equivalent diameter results in more gas to entrapped inside the expanding bubble at the orifice. Therefore, for LOX-helium systems, the size of bubbles interacting with the top free liquid surface is greater. As a result, the free liquid surface deformation for the LOX-helium is more as compared to the water-air system, Figure 5. (b).

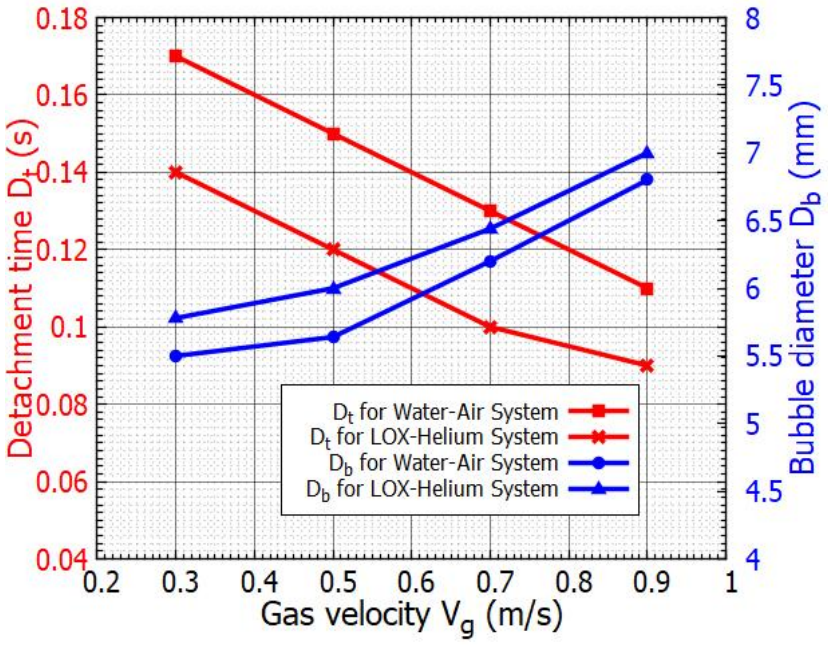

(a)

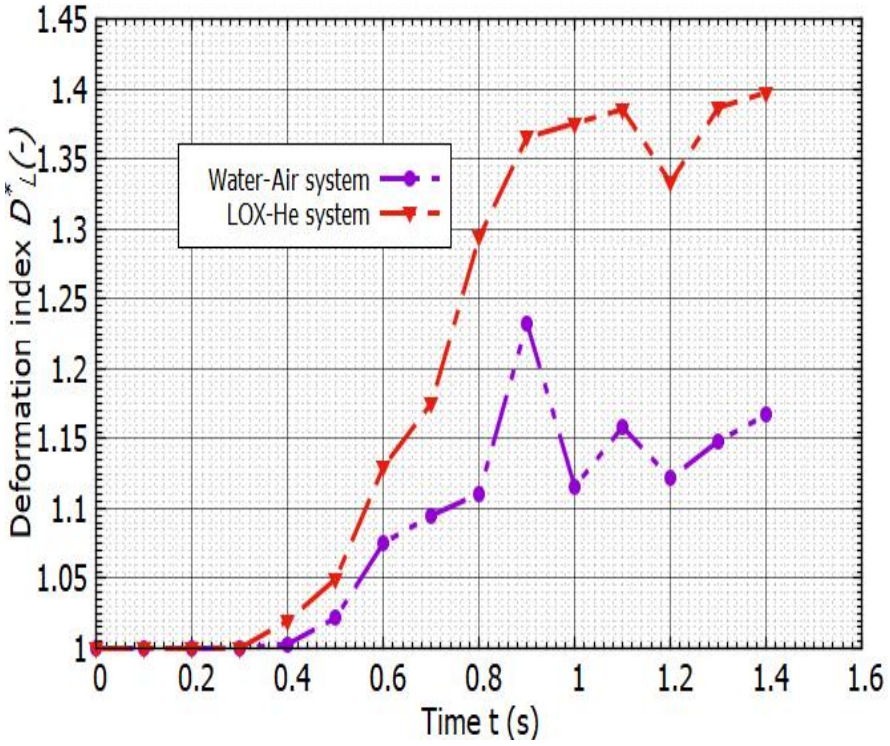

(b)

Figure 5 (a): Variation in D_t and D_b **5 (b):** Variation in deformation index

Conclusions

The VOF method of OpenFOAM is used in the current work to examine different bubble behaviors and the rupturing of free liquid surfaces due to bubbling. A 2D rectangular container was the domain that was taken into account. 15% of the domain was set aside as free space to analyze the bubble bursting at the free liquid surface. For this simulation, interFoam was employed as the solver. With the increase in inlet gas velocity detachment time for the bubble was reduced whereas the average bubble diameter values increased for both the water-air and LOX-helium systems. However, the D_b values are higher for the LOX-helium system. Qualitative results of free liquid surface bursting showed that the agitation, bursting of the bubble at the top free liquid surface, and wakening effect within the bulk is more for the LOX-helium system. Present showed that bubbles of larger diameters are formed for V_g= 0.9 m/s. The free liquid surface rupturing was found to be more for the case with V_g= 0.9 m/s. The numerical results show that the average deformation index increased by 23.83% when the water-air system was replaced with the LOX-He system. Therefore, the present analysis concludes that under a given condition the free liquid surface deformation is more for the case where storage vessels filled with LOX-He. Hence, it can be understood that for the storage vessels filled with cryogenic liquids, more safety precautions have to be considered to avoid thermal stratification. The safety precautions include increasing the gas flow rate and including more number gas flow inlets.

The current computational fluid dynamics (CFD)analysis is crucial for designing gas bubble liquid columns with the best safety performance, minimum feasible overall dimension, and lowest possible cost. The present work can be extended for the investigations incorporating optimization for getting accurate safety precaution systems for thermal destratifications in storage vessels considering the continuous supply of gases.

References

1. Sarath SR, Jayakumar JS. Bubble dynamics and deformation of the free liquid surface in aerated liquid storage tanks. Korean J Chem Eng. 2021;38(4):716-35. Available from: https://doi.org/10.1007/s11814-021-0747-y
2. Raj S, Jayakumar JS. Study of Bubble Dynamics and Free Liquid Surface Mixing in a Rectangular Container Having Ullage Area with Double Gas Inlets. Advances in Interdisciplinary Engineering. Springer. Singapore. 2019:769–81 Available from: https://doi.org/10.1007/978-981-13-6577-5_75
3. Arai E, Villafranco D, Grace S, Ryan E. Simulating bubble dynamics in a buoyant system. Int J Numer Methods Fluids. 2020;92:169-88. Available from: https://doi.org/10.1002/fld.4778
4. J Lim JH, Bae K, Shin JH, Kim DH, Lee JH, Han H, et al. Effect of particle–particle interaction on the bed pressure drop and bubble flow by computational particle-fluid dynamics simulation of bubbling fluidized beds with shroud nozzle. Powder Technology. 2016;288:315-23. Available from: https://doi.org/10.1016/j.powtec.2015.11.017
5. Choi MJ, Coleman AJ, Saunders JE. The influence of fluid properties and pulse amplitude on bubble dynamics in the field of a shock wave lithotripter. Phys Med Biol. 1993;38(11):1561-80. Available from: https://doi.org/10.1088/0031-9155/38/11/002
6. Becker A, Kapitz M, Wiesche S. Numerical Simulation of Single Bubble Dynamics During Flow Boiling Conditions on a Horizontal Surface. Heat Transf Eng. 2013;31(5):461-71. Available from: https://doi.org/10.1080/01457632.2013.833045
7. Behdani B, Monjezi S, Zhang J. Direct numerical simulation of microbubble streaming in a microfluidic device: The effect of the bubble protrusion depth on the vortex pattern. Korean J Chem Eng. 2020;37:2117–23. Available from: https://doi.org/10.1007/s11814-020-0656-5
8. Duo M, Liu M, Zu Y, Tang C. Two-dimensional volume of fluid simulation studies on single bubble formation and dynamics in bubble columns. Chem Eng Sci. 2012;72:61-77. Available from: https://doi.org/10.1016/j.ces.2012.01.013
9. Díaz ME, Iranzo A, Cuadra D, Barbero R, Montes FJ, Galán MA. Numerical simulation of the gas–liquid Flow in a laboratory scale bubble column: Influence of bubble size distribution and non-drag forces. Chem Eng J. 2008;139(2): 363-79.Available from: https://doi.org/10.1016/j.cej.2007.08.015
10. Donnelley M, Siu K, Jamison R et al. Synchrotron phase-contrast X-ray imaging reveals fluid dosing dynamics for gene transfer into mouse airways. Gene Ther. 2012;19:8–14. Available from: https://doi.org/10.1038/gt.2011.80
11. Raj S, Jayakumar JS. Simulation of Convective Heat Transfer in 3D Forward Facing Step Using Various Turbulence Models. J Eng Technol Sci. 2020;52(5):621-38. Available from: https://doi.org/10.5614/j.eng.technol.sci.2020.52.5.2
12. Sarath SR, Jayakumar JS. Thermal destratification of cryogenic liquid storage tanks by continuous bubbling of gases. Int J Hydrog Energy. 2022;47(81): 34504-32. Available from: https://doi.org/10.1016/j.ijhydene.2022.06.318
13. Raj Sarath, Jayakumar JS. Analysis of bubble dynamics and thermal destratification induced by gas bubbles in cylindrical liquid storage tanks. Therm Sci Eng Prog. 2022;36:101481. Available from: https://doi.org/10.1016/j.tsep.2022.101481
14. Hirt CW, Nichols BD. Volume of fluid (VOF) method for the dynamics of free boundaries. J Comput Phys. 1981;39(1): 201-25. Available from: https://doi.org/10.1016/0021-9991(81)90145-5
15. Raj Sarath, Jayakumar JS. Investigation of Bubble Dynamics with Single and Double Gas Inlet(s) in a Rectangular Container Using OpenFOAM. 4th National and 2nd International ISHMT-ASTFE Heat and Mass Transfer. 2017:2089-96. Available from: http://dx.doi.org/10.1615/IHMTC-2017.2930
16. Bibin KS, Jayakumar JS. Thermal hydraulic characteristics of square ducts having porous material inserts near the duct wall or along the duct centre. Int J Heat Mass Transf. 2022;131:105835. Available from: https://doi.org/10.1016/j.ijheatmasstransfer.2019.119079

17. Bibin KS, Jayakumar JS. Modelling of boiling in square channels partially filled with porous medium. Int. Commun. Heat Mass Transf. 2022;131:105835. Available from: https://doi.org/10.1016/j.icheatmasstransfer.2021.105835

18. Stavroula B. Knowledge of and attitudes to Occupational Health & Safety among tutors of a Vocational Training Institute (IIEK) in Greece: A pilot study. Int J Occup Saf Health. 2012;2(1):15-25. Available from: http://dx.doi.org/10.3126/ijosh.v2i1.5341

19. Shrestha B, Manandhar N, Joshi SK. Knowledge of occupational health hazards and practice of personal protective equipment among fabrication workers in Kathmandu district, Nepal. Int J Occup Saf Health. 2020;10 (2):1-9. Available from: https://doi.org/10.3126/ijosh.v10i2.33330

20. Banibrata D, Tirthankar G. Physical Exertion, Thermal stress affect the Cognitive Performance on Adolescent Farmers of West Bengal, India. Int J Occup Saf Health. 2018;8(2):1-6. Available from: DOI: https://doi.org/10.3126/ijosh.v8i2.23331

21. Gangopadhyay S, Effects of Interactive Environment on Occupational Health and Safety. Int J Occup Saf Health. 2019;9(1):1-2. Available from: https://doi.org/10.3126/ijosh.v9i1.25159

22. Mahato PK, Gautam B, Joshi SK. Occupational injuries sustained by caregivers in geriatric care homes of Kathmandu valley. Int J Occup Saf Health. 2019;9(1):1-5. Available from: https://doi.org/10.3126/ijosh.v9i1.25160

23. Imiete G, Kpang MBBT. Health Risk Behaviors of Employees in Selected Oil Servicing Companies in Port Harcourt. Int. J. Occup. Saf. Health. 2019;9(1):1-5. Available from: https://doi.org/10.3126/ijosh.v9i1.25163

24. Bibin KS, Raj S, Jayakumar JS, Reby Roy KE. OpenFOAM modelling of single-phase and two-phase heat transfer in square ducts partially filled with porous medium. Exp. Comput. Multiph. Flow. 2024. Available from: https://doi.org/10.1007/s42757-024-0189-y

25. Raj S, Aniyan AK, Aji A, Raj A, Mohan A, Sharon TR. Fabrication and testing of portable twin filter aqua silencer. Int. j. mech. ind. technol. 2015;3(2):177-86. https://scholar.google.com/scholar?cluster=8776234837937216556&hl=en&oi=scholarr

26. Raj Sarath, Bibin KS, Roy Reby KE, Prasad Bibin, Jayakumar J S. Analysis of Thermal Stratification Decay in Liquid Storage Tanks Using Openfoam. SSRN.2024:1-81 https://ssrn.com/abstract=4753949

27. Raj Sarath, Bibin KS, Roy Reby KE, Prasad Bibin, Jayakumar J S. Analysis of free liquid surface deformation and thermal destratification in liquid storage tanks using OpenFOAM. J. Energy Storage.2024;102:1-35. https://doi.org/10.1016/j.est.2024.113848